Effect of Surfactant Monolayer on Reduction of Fe3O4 Nanoparticles under Vacuum

ARTICLE *in* THE JOURNAL OF PHYSICAL CHEMISTRY C · NOVEMBER 2008

Impact Factor: 4.77 · DOI: 10.1021/jp8052899

THE JOURNAL OF PHYSICAL CHEMISTRY C

Article

Effect of Surfactant Monolayer on Reduction of FeO Nanoparticles under Vacuum

S. Ayyappan, G. Gnanaprakash, G. Panneerselvam, M.P. Antony, and John Philip

J. Phys. Chem. C, **2008**, 112 (47), 18376-18383 • Publication Date (Web): 05 November 2008

Effect of Surfactant Monolayer on Reduction of Fe_3O_4 Nanoparticles under Vacuum

S. Ayyappan, G. Gnanaprakash, G. Panneerselvam, M.P. Antony, and John Philip*

SMARTS, NDED, Metallurgy and Materials & Chemistry Group, Indira Gandhi Centre for Atomic Research, Kalpakkam 603 102, Tamilnadu, India

Received: June 16, 2008; Revised Manuscript Received: September 12, 2008

We study the effects of surfactant monolayer coating on the reduction of Fe_3O_4 nanoparticles under vacuum thermal annealing. Oleic acid coated and uncoated Fe_3O_4 nanoparticles were synthesized by a simple coprecipitation technique. In the temperature range of 300−700 °C, the particle size and lattice constant of uncoated Fe_3O_4 nanoparticles increased from 9 to 18 nm and from 8.357 to 8.446 Å, respectively. On further heating (above 700 °C), Fe_3O_4 decomposed into γ-Fe_2O_3 and FeO phases. In the range of 800−1000 °C, the FeO phase was predominant, and its size grew significantly from 30 to 44 nm. Conversion of oleic acid coated Fe_3O_4 phase to metallic α-Fe commenced at 500 °C and continued up to 800 °C. After vacuum annealing at 800 °C, the magnetic behavior of the sample changed from ferrimagnetic to ferromagnetic. The activation energies for the phase transitions of uncoated and oleic acid coated nanoparticles were estimated to be 30.304 and 17.349 kJ/mol, respectively. Thermogravimetric analysis (TGA) coupled with mass spectrometry revealed that, for coated nanoparticles, effluents such as H_2, CO, and CO_2 from oleic acid facilitate the reduction of Fe_3O_4 into α-Fe and FeO during vacuum thermal annealing. The interaction between the headgroup of the oleic acid and the oxygen in Fe_3O_4 is expected to lead to weakened bonding, which could result in a lower activation energy for the reduction of the surfactant-coated nanoparticles. This is a plausible reason for the precipitatation of α-Fe at lower temperature (at 500 °C) in the surfactant-coated system.

Introduction

Nanoparticles have been a topic of intense research during the past few decades because of their unique size-dependent physical properties and technological applications.[1−3] Nanometer-size particles exhibit novel physical and chemical properties and high surface-to-volume ratios. Fe_3O_4 is a well-known magnetic iron oxide that has a cubic inverse spinel structure, with oxygen forming a face-centered cubic close packing and Fe cations occupying the tetrahedral and octahedral interstitial sites. Magnetite nanoparticles and their dispersions are synthesized by different routes[4−6] and used in a variety of applications.[7−12] Dispersions of magnetic nanoparticles, popularly known as ferrofluids, are surfactant-capped magnetic nanoparticles, in the size range of less than 20 nm, dispersed in a desired liquid carrier medium. An entropic effect associated with long-chain hydrocarbons of surfactants prevents particle aggregation. Ferrofluids have been found to be excellent model systems for studying fundamental aspects such as superparamagnetism,[13,14] magnetic domain structures, magnetic−dipolar interactions,[15−17] and size-dependent physical properties[18] and for probing the weak forces acting between nanodrops and the associative behavior of polymer−surfactant interactions at droplet interfaces.[19−21] They have also very recently been used for "smart cooling" applications.[22,23]

In recent years, studies have focused on morphological changes of iron oxides, broadening of coercivity, and methods to achieve higher saturation and transition temperatures of magnetites.[24] Particularly, the polymorphic nature of iron(III) oxides, α-, β-, γ-, δ-, and ε-Fe_2O_3,[25] and phase-transition studies in the nanoscale regime have attracted much attention because of the technological applications of magnetite in many fields.[26] Factors influencing phase transitions in magnetite include particle size, reaction medium, heating rate, preparation method, and metal ion doping. When magnetite phase-transition processes occur under oxidative conditions, such as in air or O_2, the two steps involving dehydration followed by oxidative decomposition result in α-Fe_2O_3 as the final decomposition product. The phase-transition process in an inert medium such as N_2 or Ar or even in a vacuum takes place in two steps with more distinct compared to oxidative conditions.[27] Sun et al. demonstrated that as-synthesized 16-nm Fe_3O_4 nanoparticles annealed at 250 °C for 2 h can be transformed into γ-Fe_2O_3 under O_2 atmosphere. The same particles annealed at 400 °C form α-Fe nanoparticles under mixed Ar + 5% H_2 atmosphere.[28] Fe_2O_3 nanoparticles loaded in the bores of oxygenated carbon nanotubes are reduced to metallic Fe at the low temperature of 600 °C relative to the reduction at 800 °C on the outer surface of metal-coated carbon nanotubes, which is attributed to the confined environment with unique electronic properties provided by the nanotubes.[29] The interaction between the electron-deficient concave surface of the nanotubes and the anionic oxygen in Fe_2O_3 is expected to cause a weakening of the bonding in Fe_2O_3 that leads to a lower the activation energy for the reduction in the nanotube bores. Stable α-Fe nanoparticles have been reduced from hematite (α-Fe_2O_3) by heating under a hydrogen flow,[4] and α-Fe hollow fibers have been obtained by reducing α-Fe_2O_3 hollow fibers at 400 °C for 4 h under hydrogen flow.[30] Sun et al. synthesized Fe by the arc discharge method and extensively studied the microstructural and magnetic properties.[31] A recent study revealed that the organic chain plays an important role in giving rise to interfacial toughening in copper−molecular nanolayer−dielectric structures.[32] The above studies show that H_2 and C play important roles in phase-transition studies. Because these organic molecules are present in surfactants, a surfactant could provide

* To whom correspondence should be addressed. E-mail: philip@igcar.gov.in.

10.1021/jp8052899 CCC: $40.75
Published on Web 11/05/2008

insight into the reduction process. In this article, we investigate the effect of a surfactant on the phase transition of oleic acid coated Fe_3O_4.

Experimental Section

Chemicals. For the synthesis of magnetite nanoparticles, $FeSO_4 \cdot 7H_2O$, $FeCl_3 \cdot 6H_2O$, 25% aqueous NH_3, ethanol, oleic acid, 35% HCl, H_2SO_4, hexane, and acetone were obtained from E-Merck. All of the chemicals were GR grade (except hexane) and were used without any further purification. Elga water with a resistivity of 8−15 MΩ·cm was used in all experiments.

Sample Synthesis. Magnetite nanoparticles were prepared by precipitating iron salts with ammonium hydroxide. The iron salt solutions were freshly prepared with 0.8 M $FeCl_3 \cdot 6H_2O$ and 0.4 M $FeSO_4 \cdot 7H_2O$ in acidic media of HCl and H_2SO_4, respectively. These iron solutions were mixed at a 1:1 ratio under constant stirring at a speed of 1000 rpm at 70 °C. This iron stock solution was the same for both samples.

Surfactant-coated magnetite nanoparticles were obtained by addition of 30% ammonium solution in the above-mentioned iron stock solution. After the addition of alkali, the pH reached a value of 10. At this stage, the solution turned black, indicating the formation of magnetite particles. After a digestion time of 20 s, 6 mL of oleic acid was added to the above solution to coat the magnetite nanoparticles. The same pH, temperature, and stirring speed were maintained for 30 min to complete the coating process. Later, the particles were acidified with dilute HCl to separate the particles from the dispersion. The top water layer with salt impurities was discarded. The obtained surfactant-coated particles were washed with Elga water at 60 °C, until the water pH reached a value of 7, to remove ionic salt impurities trapped in or adhered to the particle coagulum. Later, the water-washed particles were dispersed in hexane. The hexane dispersion was treated with acetone to induce particle aggregation. The aggregated particles were separated by centrifugation at 2500 rpm for 30 min. Addition of acetone to hexane increases the dielectric constant of the medium, which leads to the aggregation and sedimentation of particles dispersed in hexane. However, excess acetone and repeated acetone washing also cause desorption of oleic acid from the magnetite interface because of the competition between the affinity of the carboxylate group of the oleic acid to the surface of the magnetite particle and to the organic polar solvent (acetone/hexane mixture). The washing procedure was repeated twice to eliminate excess free surfactant molecules. The oleic acid coated magnetite particles were dried at 60 °C for 2 h in inert atmosphere. The average size of the particles prepared by this method was 11 nm. The detailed preparation procedures are discussed in our earlier publications.[26,33]

Sample Characterization. A Philips X′pert MPD system equipped with the Buhler high-vacuum heating stage was used for in situ high-temperature studies under vacuum. The heating stage consisted of a thin (∼80-μm) resistance-heated tantalum foil, on top of which the finely crushed powder sample was placed uniformly. The temperature was measured with a W−Re thermocouple, which was spot welded to the bottom of the tantalum heater. The temperature was controlled to an accuracy of ±1 °C. Diffraction angles were taken from 25° to 67° (2θ) using Cu Kα radiation in the Bragg−Brentano geometry. A heating rate of 1 °C /min and a holding time of 30 min before scanning at each temperature of measurement were maintained. The specimen stage was flushed with high-purity Ar before the start of each experiment, and a vacuum level of about 10^{-5} mbar was maintained throughout the experiments. Acquisition and preliminary analysis of the data were performed by the Philips X′pert Pro software, and at a later stage, the XRD patterns were verified by comparison with JCPDS data. In the case of air-annealed Fe_3O_4 nanoparticles, a MAC Science MXP18 X-ray diffractometer was used. Diffraction angles were taken from 20° to 110° (2θ) using Cr Kα radiation ($\lambda = 2.2897$ Å).

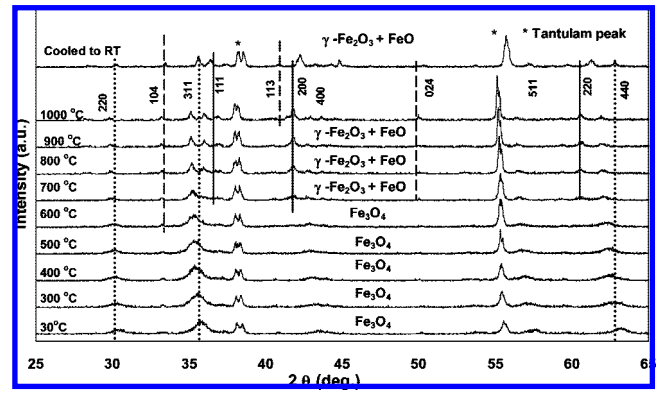

Figure 1. In situ high-temperature XRD patterns of uncoated Fe_3O_4 nanoparticles at different temperatures of 30, 300, 400, 500, 600, 700, 800, 900, and 1000 °C and cooled to room temperature. The dotted lines show the Fe_3O_4 and γ-Fe_2O_3 phases, solid lines represent the FeO phase, and dashed lines represent the α-Fe_2O_3 phase.

A Setsys Evolution-1750 Setarm instrument was used for thermogravimetric analysis (TGA) coupled with mass spectrometry (MS). Weight loss measurements were taken from 50 to 1000 °C in an inert atmosphere of argon. The effluent gases were observed using mass spectrometry by measuring the iron current. A heating rate of 5 °C/min was maintained throughout the measurements. A vibrating sample magnetometer (VSM, Lake Shore model 7404) was used for magnetization measurements with an applied magnetic field in the range of −15 to 15 kG. A Tecnai F30 instrument with an acceleration voltage of 200 kV was used to record TEM images and selected-area electron diffraction (SAED) patterns. The samples were prepared by slowly evaporating a drop of nanocrystal suspension in acetone on amorphous carbon-coated copper grids at room temperature.

Results and Discussion

Fe_3O_4 nanoparticles are heated under vacuum from room temperature to 1000 °C at regular intervals of 100 °C and cooled to room temperature. These vacuum thermal annealing XRD results are compared to those of Fe_3O_4 nanoparticles annealed under an oxidative atmosphere of air.

Phase Conversion in Uncoated Fe_3O_4 Nanoparticles. Figure 1 shows in situ high-temperature XRD patterns of uncoated Fe_3O_4 nanoparticles at different temperatures of 30, 300, 400, 500, 600, 700, 800, 900, and 1000 °C and cooled back to room temperature. The (220), (311), (400), (422), (511), and (440) diffraction peaks observed at 30 °C can be indexed to the cubic spinel structure with the Fe_3O_4 phase. The Fe_3O_4 phase is observed in the temperature range of 300−600 °C. On further heating, two distinct changes were observed. All of the observed peaks became narrower and more intense at higher temperatures, and the peaks shifted toward lower angle. The first change can be attributed to the increase in particle size due to coalescence of the particles by solid-state diffusion where the system reduces its free energy by reducing the surface area of the nanoparticles. The latter is attributed to lattice expansion with increasing temperature.

TABLE 1: Phase(s) Present, Diffraction Angle, and Particle Size of Uncoated Fe_3O_4 Nanoparticles at Different Annealing Temperatures (°C)

temperature (°C)	phase(s)	diffraction angle (deg, 2θ)	particle size (nm)
25	Fe_3O_4	35.67	9.60
300	Fe_3O_4	35.60	9.49
400	Fe_3O_4	35.47	9.94
500	Fe_3O_4	35.43	10.84
600	Fe_3O_4	35.4	12.65
700	γ-Fe_2O_3 + FeO	35.24	18.14
800	γ-Fe_2O_3 + FeO	35.19 + 41.77	34.75 + 30.39
900	γ-Fe_2O_3 + FeO	35.15 + 41.79	36.26 + 37.00
1000	γ-Fe_2O_3 + FeO	35.15 + 41.77	39.71 + 44.79
Coolto25	γ-Fe_2O_3 + FeO	35.61 + 42.14	36.3 + 35.50

TABLE 2: Phase(s) Present, Diffraction Angle, and Particle Size of Oleic Acid-Coated Fe_3O_4 Nanoparticles at Different Annealing Temperatures (°C)

temperature (°C)	phase(s)	diffraction angle (deg, 2θ)	particle size (nm)
25	Fe_3O_4	35.85	11.00
300	Fe_3O_4	35.63	12.46
500	γ-Fe_2O_3 + α-Fe	35.51 + 44.59	14.15 + 19.8
600	γ-Fe_2O_3 + α-Fe	44.57	21.48
700	α-Fe + FeO	44.51 + 41.79	25.27 + 20.26
800	α-Fe + FeO	44.43 + 41.77	30.67 + 20.75
Coolto25	α-Fe + FeO	44.87 + 42.21	28.67 + 23.67

Above 700 °C, Fe_3O_4 decomposed into γ-Fe_2O_3 and FeO phases. From 800 to 1000 °C, the XRD pattern matched the γ-Fe_2O_3 and FeO standards with additional high-intensity (110), (200), and (220) diffraction peaks. The particle sizes and lattice parameters of all of the phases are listed in Tables 1 and 2. The very low-intensity additional (104), (113), and (024) peaks confirm a small amount of α-Fe_2O_3 phase at 1000 °C. Even though the (104) peak appears above 600 °C, the remaining (113) and (024) peaks are seen only at 1000 °C. After being annealed at 1000 °C, the sample showed the peaks of FeO, γ-Fe_2O_3, and α-Fe_2O_3. The particle size of uncoated Fe_3O_4 changed from 9 to 18 nm as the temperature increased from room temperature to 700 °C. The calculated lattice constant at room temperature was 8.348 Å, which is in good agreement with the reported value of 8.39 Å.[18] The lattice constant increases from 8.348 to 8.446 Å as the temperature is increased from 300 to 600 °C, as a result of the expansion of the particle volume with temperature.

The lattice parameter and particle size growth as functions of temperature are plotted in Figure 2. Significant particle growth from 18 to 45 nm was observed as the temperature was increased from 700 to 1000 °C. The corresponding variation in the lattice constant value was from 8.459 to 4.32 Å. This reveals that Fe_3O_4 decomposed into γ-Fe_2O_3 and FeO. After the sample had been cooled to room temperature, the particle size and lattice constant of the major FeO phase were 35 nm and 4.288 Å, respectively. Because there is no oxidation atmosphere during vacuum thermal annealing, Fe_3O_4 decomposed into γ-Fe_2O_3 and FeO, and the growth of the α-Fe_2O_3 phase was suppressed during vacuum annealing. From XRD, it is difficult to distinguish magnetite from maghamite. The X-ray diffraction patterns of magnetite and maghemite phases can hardly be distinguished, as these two phases have very minor differences in diffraction (electron or X-ray) because of their identical crystal structures. However, these two phases can be easily distinguished by Mossbauer spectroscopy.[33]

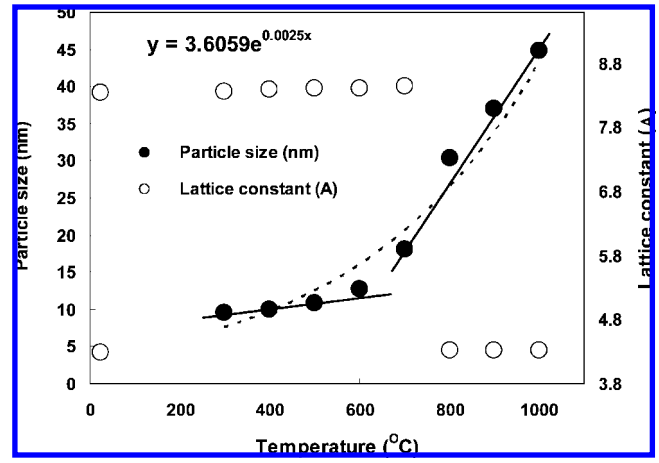

Figure 2. Variations in particle size and lattice constant of uncoated Fe_3O_4 nanoparticles at different temperatures of 30, 300, 400, 500, 600, 700, 800, 900, and 1000 °C and cooled to room temperature. The dotted line represents an exponential fit, and the straight lines show linear fits.

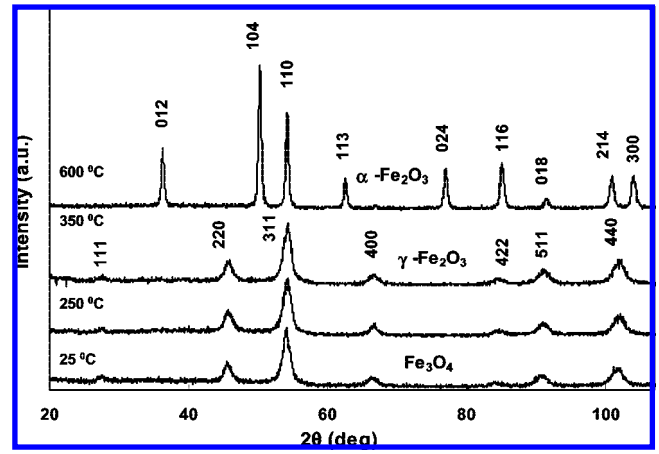

Figure 3. XRD pattern of uncoated Fe_3O_4 nanoparticles heat-treated at different oxidation temperatures of 25, 250, 350, and 600 °C in air.

To understand the role of vacuum in the phase transitions, we annealed the same samples under air atmosphere. The XRD patterns of uncoated Fe_3O_4 nanoparticles annealed in air at different temperatures of 25, 250, 350, and 600 °C are shown in Figure 3. Because Fe^{2+} ions are more sensitive to oxidation, surface ferrous ions can be oxidized to ferric ions, leading to the formation of maghemite (γ-Fe_2O_3 phase) in the temperature range of 250−350 °C. At 600 °C, the rhombohedral crystal structure of the hematite phase is evident from the characteristic (012), (104), (110), (113), (024), (116), (018), (214), and (300) peaks. Therefore, in the case of vacuum thermal annealing up to 1000 °C, uncoated Fe_3O_4 is not decomposed to hematite (α-Fe_2O_3) because of the lack of an oxidative atmosphere.

To understand the mechanism of phase transformation, gas effluents released at regular intervals during the heating process for uncoated Fe_3O_4 nanoparticles were analyzed by TGA-coupled mass spectrometry. The weight loss and evolved gases as functions of temperature are shown in Figure 4. The TGA curve of the uncoated Fe_3O_4 shows a broad one-step weight loss of 4% in the temperature range of 150−300 °C due to the moisture content in the sample. CO_2 gas evolved in the temperature range of 300−400 °C caused a weight loss of 4% for the uncoated Fe_3O_4.

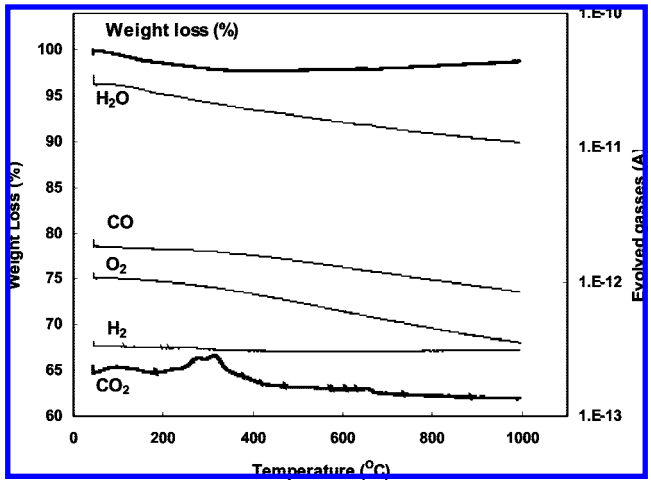

Figure 4. Weight loss and evolved gases as functions of temperature measured by TGA-coupled mass spectrometry of uncoated Fe_3O_4 nanoparticles. The heating rate was 5 °C/min.

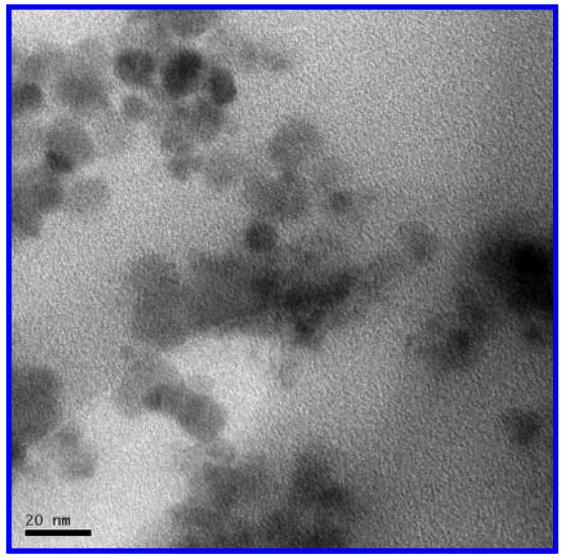

Figure 5. TEM image of oleic acid coated magnetite nanoparticles. The scale bar is 20 nm.

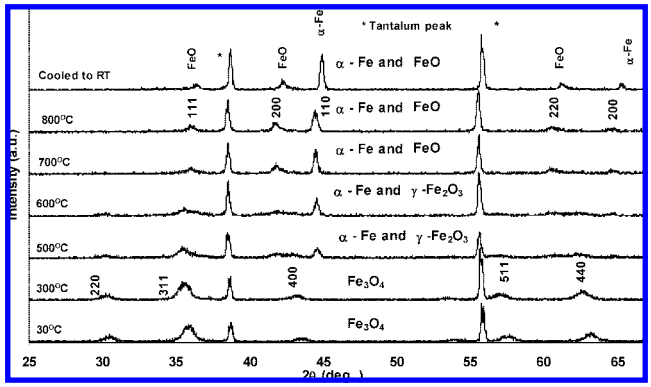

Figure 6. XRD patterns of oleic acid coated Fe_3O_4 nanoparticles at different temperatures of 30, 300, 400, 500, 600, 700, and 800 °C and cooled to room temperature.

Phase Transition in Coated Fe_3O_4 Nanoparticles. A typical TEM image of oleic acid coated Fe_3O_4 nanoparticles is shown in Figure 5. The average size of the particles is 8.2 ± 1.7 nm.

Figure 6 shows in situ high-temperature XRD patterns of the oleic acid coated Fe_3O_4 nanoparticles at different temperatures of 30, 300, 400, 500, 600, 700, and 800 °C and cooled to room temperature. The observed diffraction peaks, in the temperature range of 300−500 °C, for the (220), (311), (400), (511), and (440) planes are assigned to the cubic spinel structure of Fe_3O_4. In the temperature range of 600−800 °C, the XRD pattern matches that of α-Fe, with additional (110) and (200) peaks.

Above 700 °C, apart from the characteristic peaks of α-Fe, the additional very low-intensity (111), (200), and (220) peaks indicate the presence of the FeO phase. During the temperature rise from room temperature to 500 °C, the oleic acid coated Fe_3O_4 nanoparticle size increased from 11 to 14 nm. From 500 °C, α-Fe started to precipitate, and significant particle growth was observed up to 800 °C.

For the temperature range of 500−600 °C, the observed changes in the particle size and lattice parameter were from 14 to 21 nm and from 8.384 to 2.87 Å, respectively. The temperature-dependent particle size and lattice parameter are plotted in Figure 7. After the sample had been cooled from 800 °C to room temperature, the observed particle size and lattice parameter were 28.6 nm and 2.856 Å, respectively. Above 500 °C, oleic acid started to decompose, leading to the release of CO and CO_2 and hydrogen vapor, as confirmed by TGA-coupled mass spectrometry (Figure 8). The size and distribution of the particles have a role on the phase transitions. Although the former aspect was studied recently,[26] the latter effect has not yet been studied because obtaining information about the

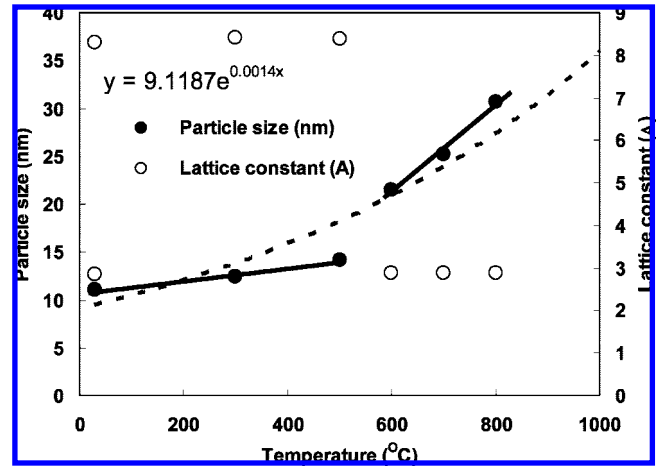

Figure 7. Particle size and lattice parameter at different temperatures of 30, 300, 400, 500, 600, 700, and 800 °C for oleic acid coated Fe_3O_4 nanoparticles annealed under a vacuum. The dotted line represents an exponential fit, and the straight lines show linear fits.

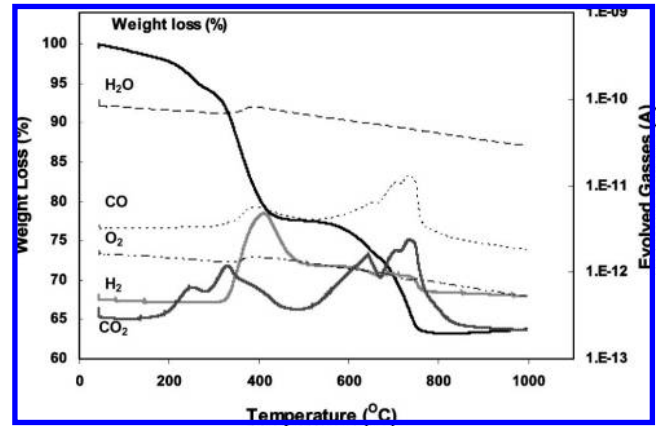

Figure 8. Thermogravimetric curve and mass spectroscopic curves of oleic acid coated Fe_3O_4 nanoparticles under inert argon atmosphere.

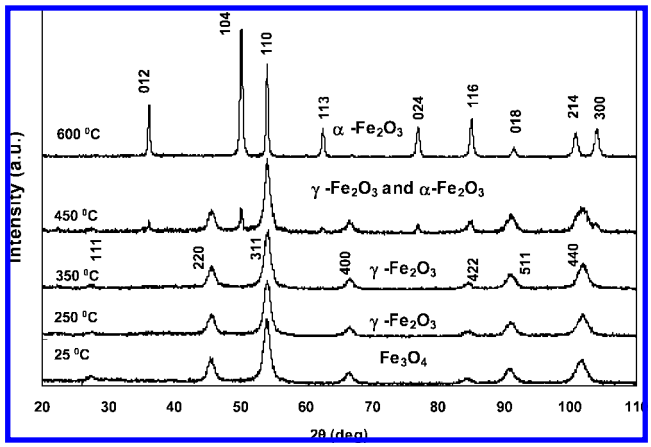

Figure 9. XRD pattern of oleic acid coated Fe_3O_4 nanoparticles heat-treated at different oxidation temperatures of 25, 250, 350, 450, and 600 °C in air.

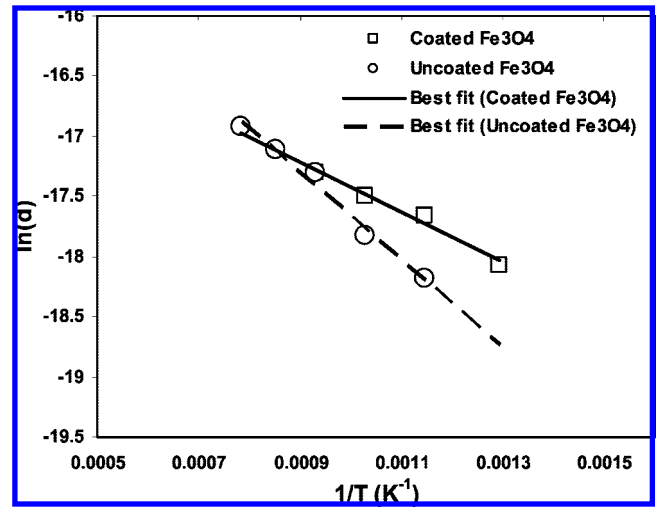

Figure 10. Plot of ln(d) versus 1/T for oleic acid coated and uncoated Fe_3O_4 nanoparticles annealed under a vacuum.

polydispersity during annealing is difficult. Further, it should be noted that the sintered particles could be polycrystalline, and hence, there could be uncertainty in the estimation of the average particle size by XRD at elevated temperatures.

Above 500 °C, the magnetite content is reduced to α-Fe. There is no indication of the FeO phase below 500 °C. The possible reduction mechanism above 600 °C is as follows

$$Fe_3O_4 + CO \rightarrow 3FeO + CO_2 \quad (1)$$

$$3FeO \Leftrightarrow Fe_2O_3 + \alpha\text{-Fe} \quad (2)$$

$$CO + \frac{1}{2}O_2 \Leftrightarrow CO_2 \quad (3)$$

It is possible that carbon from the oleic acid is oxidized (by taking oxygen from the sample) to CO and CO_2 during vacuum thermal annealing. The TGA-coupled mass spectrometry results show the presence of CO and CO_2 around 800 °C. All of the above three reactions are supported by the TGA-coupled mass spectrometry and XRD results. Therefore, in the case of oleic acid coated nanoparticles, carbon from the oleic acid causes the reduction above 500 °C under vacuum. However, for an oxidation atmosphere such as air, nonmagnetic α-Fe_2O_3 nanoparticles were observed above 600 °C,[26] as seen in Figure 9. In oxidative medium as well, both C and H_2 are released from oleic acid at temperatures above 300 °C. These evolved gases (H_2 and C) make use of freely available oxygen from the atmosphere instead of taking it from the sample, as the former is energetically favorable at atmospheric pressure. Therefore, the maghemite-to-hematite conversion started at 450 °C and was fully complete at 600 °C without the formation of metallic Fe. The rhombohedral crystal structure of hematite is evident from the major characteristic (012), (104), (110), (113), (024), (116), (018), (214), and (300) peaks, as shown in Figure 9. Therefore, the phase transition of Fe_3O_4 to α-Fe is mainly due to carbon that comes from the oleic acid surfactant during vacuum thermal annealing at temperatures above 500 °C. Earlier, Cao et al. showed that carbon in carbon nanotubes acts as a reductant in reducing Fe_3O_4 into metallic Fe for Fe_3O_4 nanowires loaded in the cavities of carbon nanotubes at temperatures around 570 °C.[34] Similarly, Hermanek et al. reported the thermal decomposition behavior of $FeC_2O_4 \cdot 2H_2O$ due to the presence of C in the inert atmosphere.[27]

To understand the reduction mechanism, gas effluents released during thermal decomposition of the oleic acid coated Fe_3O_4 nanoparticles were analyzed by TGA-coupled mass spectrometry where the sample was heated at 5 °C/min. The oleic acid coated magnetite nanoparticles exhibited a four-step weight loss in the TGA measurements. The initial weight loss of about 4% in the temperature range of 100−200 °C was due to moisture content in the sample. The second weight loss occurring at 231 °C was due to the breaking of weakly bound functional groups (COOH) from secondary and primary surfactant layer. CO_2 fractions ($m/e \approx 44$) started to evolve before 200 °C and reached their maximum at around 240 and 330 °C. H_2 ($m/e \approx 2$) became the apparent gas product from linear hydrocarbon chains along with CO ($m/e \approx 28$) after 320 °C and reached its maximum at 400 °C accompanied by a small amount of water vapor possibly produced by the reaction between H_2 and CO_2.[34] In the temperature range of 300−500 °C, the weight loss was nearly 20% and was due to the oleic acid decomposition. The third weight loss at 614 °C was from CO_2 effluents, and the fourth loss at 680 °C was mainly from CO and CO_2 effluents from the sample. The 12% weight loss in the range of 600−800 °C was due to the reduction of Fe_3O_4 to α-Fe with a small amount of FeO. These results are consistent with the XRD data, according to which α-Fe starts precipitate at 500 °C. These results show that carbon from oleic acid has a major role in reducing γ-Fe_2O_3 to α-Fe at 600 °C during vacuum annealing.

For a close-packed monolayer of surfactant on the surface of spherical nanoparticles of diameter d, oleic acid molecules occupy a surface area a, and the surface area per particle is πd^2. The total number of particles, N, is then given by

$$N = \frac{(100 - W)}{\rho(\pi d^3/6)} \quad (4)$$

where W is the weight of the surfactant in percentage (obtained from TGA) and ρ is the density of the particle. The total number of surfactant molecules in the system is WN_0/M, where N_0 is Avogadro's number and M is the molecular weight of the surfactant. Therefore, the surface area a occupied by oleic acid molecules is the ratio of the total surface area of the particles to the number of surfactant molecules

$$a = \frac{6(100 - W)M}{N_0 d\rho W} \quad (5)$$

The calculated surface area of oleic acid molecules on magnetite surface is 0.24 nm^2 (for $W = 20\%$, $M = 282$ g/mol, $d = 9.8$ nm, and $\rho = 5.18$ g/cm^3). This value is in good agreement with

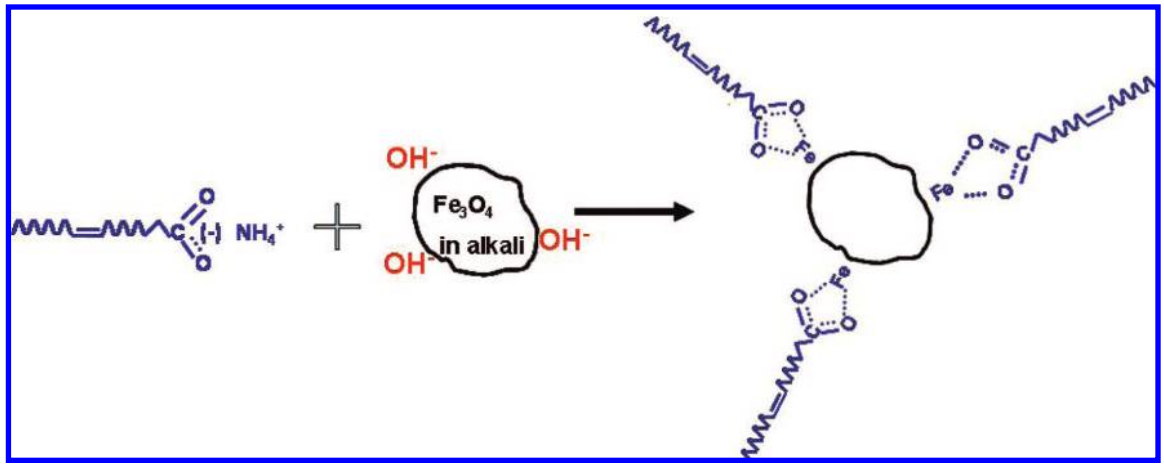

Figure 11. Schematic diagram of oleic acid coated Fe_3O_4 nanoparticles.

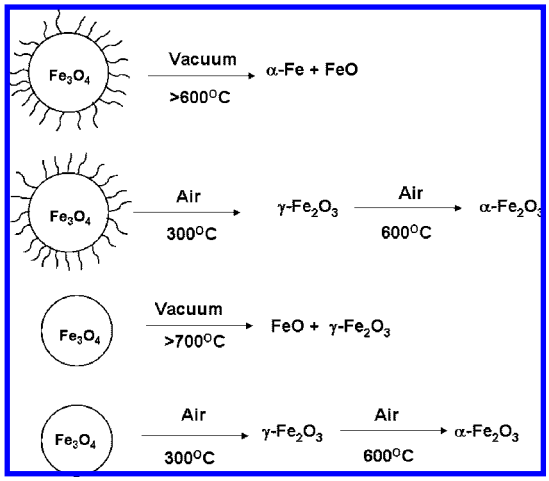

Figure 12. Schematic of the phase transitions in coated and uncoated magnetite nanoparticles under vacuum and air annealing.

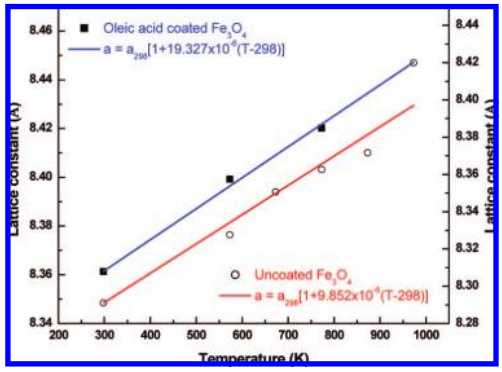

Figure 13. Variations of the lattice parameters of oleic acid coated and uncoated Fe_3O_4 nanoparticles under vacuum thermal annealing.

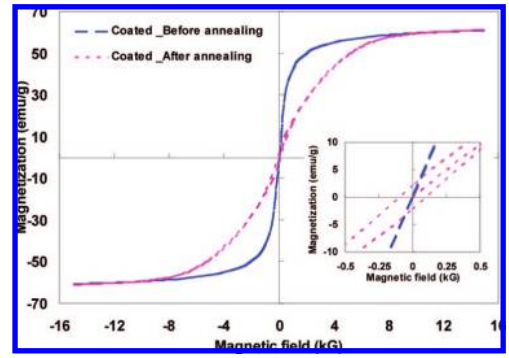

Figure 14. Hysteresis loop of oleic acid coated Fe_3O_4 nanoparticles at room temperature and fields up to 15 kG for a sample annealed at 800 °C. The inset shows an expanded view of the hysteresis loop at low field.

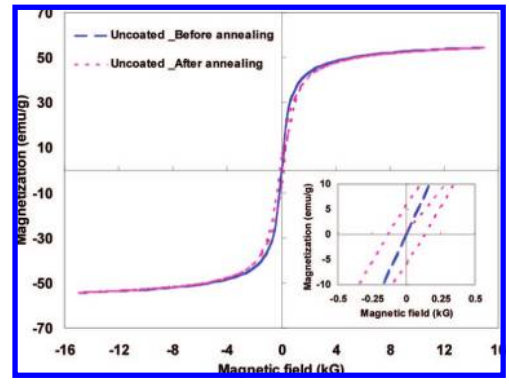

Figure 15. Hysteresis loop of uncoated Fe_3O_4 nanoparticles at room temperature and fields up to 15 kG for a sample annealed at 1000 °C. The inset shows an expanded view of the hysteresis loop at low field.

the reported values of 0.28 and 0.3 nm^2 for particles of nearly 10 nm coated with oleic acid as a monolayer.[33,35] If there were several surfactant layers, the weight loss would have been more than 20%.

The homogeneous growth rate during vacuum thermal annealing of nanoparticles is given by the Schott equation[36]

$$d = A \exp\left(\frac{-E}{RT}\right) \quad (6)$$

where d is the particle size, A is a constant, E is the activation energy for crystal growth, R is the ideal gas constant, and T is the absolute temperature.

Figure 10 shows the variation of particle size [ln(d)] with inverse temperature (1/T) for oleic acid coated and uncoated Fe_3O_4 nanoparticles. The activation energy (E) of the phase transition for oleic acid coated and uncoated Fe_3O_4 nanoparticles was estimated by the Schott equation to be 17.349 and 30.304 kJ/mol, respectively. In the coating process, the oleate anions replace the magnetite-surface-bound OH^- ions by ion-exchange adsorption. The fatty acid coating on the iron oxide particles is weakly adsorbed, possibly by electrostatic forces.[37] The negative charge at the carboxylate ion of oleic acid delocalizes between the two oxygen atoms because of the resonance effect, which is schematically shown in Figure 11. Therefore, the interaction

between the headgroup of the oleic acid and the oxygen in Fe_3O_4 could lead to weakening of the bonding in Fe_3O_4, which could, in turn, lead to a lower activation energy for the reduction of oleic acid coated Fe_3O_4 compared to the uncoated particles. This is a plausible reason for the early precipitatation of α-Fe (at 500 °C) in the surfactant-coated system. The reduction in metal oxides is governed by nucleation-controlled processes that involve uniform internal reduction and occur by the initial random removal of lattice oxygen atoms until a critical concentration of vacancies is reached. The annihilation of vacancies by lattice rearrangement produces metal nuclei. The reduction process accelerates because of the increasing metal−metal oxide interface that is further increased by the formation of new nuclei. The merging of product nuclei causes a decrease in sample−product interfacial area.[38] The activation energy of $ZnFe_2O_4$ nanoparticles growth during vacuum thermal annealing over a temperature range of 600−1000 °C was found to be 18.20 kJ/mol, where the crystal growth is attributed to the coalescence of particles by solid-state diffusion.[39] In the case of $NiFe_2O_4$ nanoparticles during calcination over a temperature range of 600−800 °C, the activation energy was found to be 16.6 kJ/mol, where the crystal growth is expected to be due to an interfacial reaction.[40] Earlier studies showed that the initial particle size has a major influence on the activation energy.[26]

Schemes of various phase transformations under air and vacuum for coated and uncoated samples are shown in Figure 12.

Figure 13 shows the variation of the lattice parameter with increasing temperature for oleic acid coated and uncoated Fe_3O_4 nanoparticles under vacuum thermal annealing. The lattice expansion with increasing temperature is a well-known phenomenon.[41] The lattice parameter data of oleic acid coated and uncoated Fe_3O_4 nanoparticle were fitted to a second-degree polynomial in the temperature increment to deduce the thermal expansion of the materials. From the lattice parameter, the instantaneous (α_i), mean (α_m), and relative (α_r) linear thermal expansion coefficients were estimated. From the above XRD patterns, the lattice parameters calculated for oleic acid coated and uncoated Fe_3O_4 nanoparticles at room temperature were 8.3078 and 8.3484 Å, respectively, which is in a good agreement with reported values of normal spinel structured Fe_3O_4.[18] For the coated and uncoated Fe_3O_4 nanoparticles, the temperature-dependent lattice parameter data could be fitted by the expressions $a = a_{298}[1 + 19.327 \times 10^{-6}(T - 298)]$ and $a = a_{298}[1 + 9.852 \times 10^{-6}(T - 298)]$, respectively, where a_{298} is the unit cell dimension of Fe_3O_4 nanoparticles at room temperature ($T = 293$ K). The coefficients of mean linear thermal expansion of oleic acid coated and uncoated Fe_3O_4 nanoparticles were determined experimentally to be 19.327×10^{-6} and 9.852×10^{-6} K^{-1}, respectively, which are quite similar to the value reported for $ZnFe_2O_4$ nanoparticles (7.1×10^{-6} K^{-1}).[39]

Figures 14 and 15 show the hysteresis loop before and after vacuum thermal annealing for coated and uncoated Fe_3O_4 nanoparticles, respectively. When the particles are single-domain (for Fe_3O_4, ~28 nm), they exhibit ferrimagnetic behavior. Particles exhibit superparamagnetic behavior above the blocking temperature as a result of the suppression of Weiss anisotropy constant. Before thermal annealing, both samples showed superparamagentic behavior with zero coercivity and remanance. After vacuum thermal annealing, the oleic acid coated Fe_3O_4 nanoparticles showed minimum hysteresis of 50 G in their magnetization data at 290 K (Figure 15). After annealing at 1000 °C, the uncoated Fe_3O_4 sample was converted from ferri- to ferromagnetic with a hysteresis of 200 G. However, the saturation magnetization of the sample remained the same because of the dominance of γ-Fe_2O_3. In the case of oleic acid coated Fe_3O_4 nanoparticles, after thermal annealing, the sample was converted from ferrimagnetic to ferromagnetic. However, the saturation magnetization field after annealing was much higher (9 instead of 3 kG) because of the presence of α-Fe and FeO phases. Before and after vacuum thermal annealing, the saturation magnetization of oleic acid coated Fe_3O_4 nanoparticle was around 61 emu/g at 290 K. In the magnetization calculations, we considered only the particle weight. The saturation magnetization value of standard crystalline α-Fe is nearly 220 emu/g at 298 K,[42,43] whereas the value for bulk amorphous Fe is about 156 emu/g. Even though we observed that α-Fe started to precipitate at 500 °C, the magnetization was only one-third of its bulk value of 220 emu/g. The presence of the FeO phase, which is paramagnetic at room temperature, and decomposed carbon from oleic acid reduced the net saturation magnetization after vacuum thermal annealing.

Conclusions

The effect of a surfactant monolayer on the reduction of Fe_3O_4 nanoparticles under vacuum and air thermal annealing was studied using high-temperature XRD. The results showed that uncoated Fe_3O_4 nanoparticles are converted to a mixed phase of γ-Fe_2O_3 and FeO after heat treatment at 1000 °C. In the case of oleic acid coated magnetite nanoparticles, metallic α-Fe starts to precipitate at 500 °C, and significant particle growth occurs as the annealing temperature increases up to 800 °C. A mixed phase of α-Fe and FeO was observed even after cooling to the room temperature. The α-Fe_2O_3 phase was observed for both coated and uncoated Fe_3O_4 nanoparticles after annealing at 600 °C under oxidation atmosphere such as air. TGA-coupled mass spectra of oleic acid coated Fe_3O_4 nanoparticles showed that hydrogen and carbon from the surfactant species are converted into H_2O, CO, and CO_2 gases by taking oxygen from the sample. Therefore, carbon from the surfactant species is responsible for the reduction of oleic acid coated Fe_3O_4 into metallic α-Fe above 600 °C. The interaction between the headgroup of the oleic acid and the oxygen in Fe_3O_4 is expected to cause weakened bonding that could result in a lower activation energy for the reduction of oleic acid coated nanoparticles. This is a plausible reason for the precipitatation of α-Fe at lower temperature (at 500 °C) in the surfactant-coated system. After vacuum annealing at 800 °C, the magnetic behavior of the sample changed from ferri- to ferromagnetic. In the case of uncoated Fe_3O_4, no dramatic change in magnetization values was observed before and after annealing under vacuum because of the presence of the γ-Fe_2O_3 phase.

Acknowledgment. We thank Dr. T. Jayakumar, Dr. P. R.Vasudeva Rao, and Dr. Baldev Raj for their support and encouragement. We also thank Dr. R. Sridharan for TGA/MS measurements.

References and Notes

(1) Wang, X.; Zhuang, J.; Peng, Q.; Li, Y. *Nature* **2005**, *437*, 3968.
(2) Klabunde, K. J. *Nanoscale Materials in Chemistry*; John Wiley & Sons Inc.: New York, 2001.
(3) Rao, C. N. R.; Muller, A.; Cheetham, A. K. *The Chemistry of Nanomaterials*; Wiley-VCH: Weinheim, Germany, 2004; Vol. 1.
(4) Santos, F. J.; Varanda, L. C.; Ferracin, L. C. *J. Phys. Chem. C* **2008**, *112*, 5301.
(5) Zou, G.; Xiong, K.; Jiang, C.; Li, H.; Li, T.; Du, J.; Qian, Y. *J. Phys. Chem C* **2005**, *109*, 18356.
(6) Xu, L.; Zhang, W.; Ding, Y.; Peng, Y.; Zhang, S.; Yu, W.; Qian, Y. *J. Phys. Chem. C* **2004**, *108*, 10859.

(7) Resendez, R. M.; Morales, M. P.; Serna, C. J. *Mater. Sci. Eng. C* **2003**, *23*, 1139.
(8) Bader, S. D. *Rev. Mod. Phys.* **2006**, *78*, 1.
(9) Pankhurst, Q. A.; Connolly, J.; Jones, S. K.; Dobson, J. *J. Phys. D Appl. Phys.* **2003**, *36*, R167.
(10) Pankhurst, Q. A.; Pollard, R. J. *J. Phys.: Condens. Matter* **1993**, *3*, 8487.
(11) Lacava, L. M.; Garcia, V. A. P.; Kuckelhaus, S.; Azevedo, R. B.; Lacava, Z. G. M.; Silva, O.; Pelegrini, F.; Gansau, C.; Buske, N.; Morais, P. C. *J. Appl. Phys.* **2003**, *93*, 7563.
(12) Perez, J. M.; O'Loughin, T.; Simeone, F. J.; Weissleder, R.; Josephson, L. J. *Am. Chem. Soc.* **2002**, *124*, 2856.
(13) Song, Q.; Zhang, Z. J. *J. Phys. Chem. B* **2006**, *110*, 11205.
(14) Hrianca, I.; Caizer, C.; Schlett, Z. *J. Appl. Phys.* **2002**, *92*, 2125.
(15) Tronc, E.; Ezzir, A.; Cherkaoui, R.; Chaneac, C.; Nogues, M.; Kachkachi, H.; Fiorani, D.; Testa, A. M.; Greneche, J. M.; Jolivet, J. P. *J. Magn. Magn. Mater.* **2000**, *221*, 63.
(16) Vestal, C. R.; Zhang, Z. J. *J. Am. Chem. Soc.* **2003**, *125*, 9828.
(17) Dormann, J. L.; Spinu, L.; Tronc, E.; Jolivet, J. P.; Lucari, F.; D'Orazio, F.; Fiorani, D. *J. Magn. Magn. Mater.* **1998**, *183*, L255.
(18) He, Y. P.; Miao, Y. M.; Li, C. R.; Wang, S. Q.; Cao, L.; Xie, S. S.; Yang, G. Z.; Zou, B. S. *Phys. Rev. B* **2005**, *71*, 125411.
(19) Philip, J.; Gnanaprakash, G.; Jayakumar, T.; Sundaram, P. K.; Raj, B. *Phys. Rev. Lett.* **2002**, *89*, 268301.
(20) Philip, J.; Gnanaprakash, G.; Jayakumar, T.; Sundaram, P. K.; Monval, O. M.; Raj, B. *Langmuir* **2002**, *18*, 4625.
(21) Philip, J.; Gnanaprakash, G.; Jayakumar, T.; Sundaram, P. K.; Raj, B. *Macromolecules* **2003**, *36*, 9230.
(22) Philip, J.; Shima, P. D.; Raj, B. *Appl. Phys. Lett.* **2007**, *91*, 203108.
(23) Philip, J.; Shima, P. D.; Raj, B. *Appl. Phys. Lett.* **2008**, *92*, 043108.
(24) Zhao, L.; Zhang, H.; Xing, Y.; Song, S.; Yu, S.; Shi, W.; Guo, X.; Yang, J.; Lei, Y.; Cao, F. *Chem. Mater.* **2007**, *20*, 198.
(25) Zboril, R.; Mashlan, M.; Petridis, D. *Chem. Mater.* **2002**, *14*, 969.
(26) Gnanaprakash, G.; Ayyappan, S.; Jayakumar, T.; Philip, J.; Raj, B. *Nanotechnology* **2006**, *17*, 5851.
(27) Hermanek, M.; Zboril, R.; Mashlan, M.; Machala, L.; Schneeweiss, O. *J. Mater. Chem.* **2006**, *16*, 123.
(28) Sun, S.; Zeng, H. *J. Am. Chem. Soc.* **2002**, *124*, 8204.
(29) Chen, W.; Pan, X.; Willinger, M-G.; Su, D. S.; Bao, X. *J. Am. Chem. Soc.* **2006**, *128*, 3136.
(30) Zhan, S.; Chen, D.; Jiao, X.; Liu, S. *J. Colloid Interface Sci.* **2007**, *308*, 265.
(31) Sun, X. C.; Nava, N. *Nano Lett.* **2002**, *2*, 765.
(32) Gandhi, D. D.; Lane, M.; Zhou, Y.; Singh, A. P.; Nayak, S.; Tisch, U.; Eizenberg, M.; Ramanath, G. *Nature* **2007**, *447*, 299.
(33) Gnanaprakash, G.; Philip, J.; Jayakumar, T.; Raj, B. *J. Phys. Chem. B* **2007**, *111*, 7978.
(34) Cao, F.; Zhong, K.; Gao, A.; Chen, C.; Li, Q.; Chen, Q. *J. Phys. Chem. B* **2007**, *111*, 1724.
(35) van Ewijk, G. A.; Vroege, G. J.; Philipse, A. P. *J. Magn. Magn. Mater.* **1999**, *201*, 31.
(36) Scott, M. G. *Amorphous Metallic Alloys*; Butterworths: London, 1983.
(37) Fried, T.; Shemer, G.; Markovich, G. *Adv. Mater.* **2001**, *13*, 1158.
(38) Tiernan, M. J.; Barnes, P. A.; Parkesre, G. M. B. *J. Phys. Chem. B* **2001**, *105*, 220.
(39) Philip, J.; Gnanaprakash, G.; Panneerselvam, G.; Antony, M. P.; Jayakumar, T.; Raj, B *J. Appl. Phys.* **2007**, *102*, 054305.
(40) Yang, H.; Zhang, X.; Ao, W.; Qiu, G. *Mater. Res. Bull.* **2004**, *39*, 833.
(41) Sepelak, V.; Wilde, L.; Steinike, U.; Becker, K. D. *Mater. Sci. Eng. A* **2004**, *375*−*377*, 865.
(42) Cullity, B. D. *Introduction to Magnetic Materials*; Addison-Wesley: New York, 1972.
(43) Suslick, K. S.; Fang, M.; Hyeon, T. *J. Am. Chem. Soc.* **1996**, *118*, 11960.

JP8052899